

# Analyses of Core Plasma Confinement and Internal Transport Barrier Formation in Tokamak and Helical Reactors<sup>\*)</sup>

Tomoyuki YAMAKAMI, Kozo YAMAZAKI, Hideki ARIMOTO and Tatsuo SHOJI

*Nagoya University, Furo-cho, Chikusa-ku, Nagoya 464-8603, Japan*

(Received 6 December 2012 / Accepted 11 April 2013)

High performance operation with Internal Transport Barrier (ITB) is effective to improve the core plasma confinement in the future fusion reactor. Numerous plasma experiments with ITB were confirmed in the reversed magnetic shear. It is considered that ITB formation could be controlled by external fueling. In this study, firstly, the feasibility of pellet injection condition is simulated in tokamak reactor. Secondly, the effect of the pellet injection on the core plasma profile and ITB formation is analyzed at tokamak and helical reactors. Simulations are carried out using the toroidal transport linkage code TOTAL. In case of the operation with pellet injection from high magnetic-field side (HFS), the feasibility of pellet injection condition for ITB formation is demonstrated in the ITER-like tokamak reactor, TR-1. In both tokamak and helical reactors, it is shown that pellet injection depth is not related to the position of ITB formation, but it has significant effect to the radial profile. In helical case, wide-ranged ITB is formed when the pellet is injected centrally.

© 2013 The Japan Society of Plasma Science and Nuclear Fusion Research

Keywords: internal transport barrier, magnetic shear, pellet injection, tokamak reactor, helical reactor

DOI: 10.1585/pfr.8.2403079

## 1. Introduction

The improvement of core plasma confinement is one of important topics for fusion reactor research and development. In future reactors, it is difficult to control plasma temperature and current density profiles only by external heating and current drive methods since self-burning mechanism is expected as a main process of plasma heating. Therefore, to optimize the core plasma condition, it is important to control the plasma density fueling externally through internal transport processes. In various tokamak operations, it is confirmed that the internal transport barrier (ITB) is formed by using the operation scenario with negative magnetic shear. When ITB is formed, it is expected that plasma confinement will be highly improved and temperature and density in the core plasma region will be increased because the local high pressure gradient is considered to be obtained by the suppression of ITG turbulence due to  $E \times B$  shear flow near zero-shear region. Therefore, the operation with ITB formation is expected in attractive future reactors. The ITB formation could be controlled by the density control of the core plasma by fueling. For understanding the mechanism of ITB, it is important to study how density control has an effect on the ITB formation. As a method of central fueling, pellet injection from magnetic high-field side (HFS) is one of promising methods. The ITB model based on Bohm and Gyro-Bohm-like transport model with  $E \times B$  shear flow effects has already been compared with the JET experimental ITB in

tokamak systems [1] and with the LHD experimental ITB in helical systems [2]. This model is introduced into the toroidal transport linkage TOTAL code [3, 4], and is applied to the one-dimensional ITB formation simulation of both 3-D equilibrium helical and 2-D equilibrium tokamak plasmas.

Section 2 will describe the details of the transport model and pellet ablation model. Simulation result will be described in section 3, and the conclusion is given in section 4.

## 2. Calculation Models

### 2.1 Transport model

The most widely accepted explanation for ITB formation relies on the suppression of ITG turbulence due to  $E \times B$  shear flow. The suppression of turbulence might occur when the  $E \times B$  flow shearing rate  $\omega_{E \times B}$  exceeds the ITG linear growth rate  $\gamma_{ITG}$ . The shearing rate  $\omega_{E \times B}$  is defined as [5, 6]

$$\omega_{E \times B} \cong \left| \frac{RB_\theta}{B_\phi} \frac{\partial}{\partial r} \left( \frac{E_r}{RB_\theta} \right) \right|, \quad (1)$$

where  $E_r$ ,  $B_\theta$  and  $B_\phi$  are the radial electric field, poloidal and toroidal magnetic fields, respectively. In tokamak plasmas, the radial electric field  $E_r$  is not easily determined, but can be calculated from the plasma radial force balance equation under the assumption that the toroidal and poloidal velocities can be expressed according to the neo-classical theory [7, 8]. However, in this paper,  $E_r$  is de-

author's e-mail: yamakami.tomoyuki@a.mbox.nagoya-u.ac.jp

<sup>\*)</sup> This article is based on the presentation at the 22nd International Toki Conference (ITC22).

scribed simply as

$$\frac{dE_r}{dr} \cong -\frac{1}{en_i^2} \frac{dn_i}{dr} \frac{dp_i}{dr}, \quad (2)$$

in the H-mode tokamak condition [9], where  $n_i$  and  $p_i$  are ion density and ion pressure, respectively. On the other hand, in helical plasmas, the radial electric field  $E_r$  is determined by ambipolar condition [3]

$$\Gamma_i = \Gamma_e, \quad (3)$$

where  $\Gamma_i$  and  $\Gamma_e$  are neoclassical ion particle flux and electron particle flux respectively. The ITG growth rate  $\gamma_{\text{ITG}}$  is defined as [10]

$$\gamma_{\text{ITG}} = \frac{(\eta_i - 2/3)^{1/2} |s| c_i}{qR}, \quad (4)$$

where  $\eta_i = L_n/L_T$ ,  $L_n^{-1} = -\nabla n/n$ ,  $L_T^{-1} = -\nabla T_i/T_i$ ,  $c_i = (T_i/m_i)^{1/2}$  and  $q$  is the safety factor,  $s$  is the magnetic shear which is defined as

$$s = \frac{r}{q} \left( \frac{dq}{dr} \right). \quad (5)$$

In the present studies based on the  $E \times B$  shear stabilization, thermal diffusion coefficient  $\chi$  is usually described as

$$\chi_{e,i} = \chi_{\text{neoclassical}} + \chi_{\text{anomalous}}, \quad (6)$$

$$\chi_{\text{anomalous}} = (\alpha_1 \times \chi_{\text{Gyrobohm}} + \alpha_2 \times \chi_{\text{Bohm}}) \times F(\omega_{E \times B}/\gamma_{\text{ITG}}), \quad (7)$$

where stabilization factor  $F(\omega_{E \times B}/\gamma_{\text{ITG}})$  is described as

$$F(\omega_{E \times B}/\gamma_{\text{ITG}}) = \frac{1}{1 + \tau(\omega_{E \times B}/\gamma_{\text{ITG}})^\gamma}. \quad (8)$$

The coefficient  $\chi_{\text{neoclassical}}$  is the neoclassical part of the thermal diffusion coefficient, and  $\chi_{\text{anomalous}}$  is the anomalous part described in the Bohm and Gyro-Bohm mixed transport model described in ref [1, 2]. In this study, we used  $\alpha_1 = 0.5$ ,  $\alpha_2 = 4.0$ ,  $\tau = 2.0$  and  $\gamma = 4.0$  in tokamak case, and  $\alpha_1 = 5.0$ ,  $\alpha_2 = 0.2$ ,  $\tau = 15.0$  and  $\gamma = 2.0$  in helical case. These parameters are decided from the comparison between simulation results using TOTAL code and the experimental data of JT-60U and LHD [11–13].

## 2.2 Pellet Injection Model

The pellet injection consists of two processes; pellet ablation and mass relocation. In this study, the pellet injection from the high-field side (HFS) is simulated by combining the pellet ablation model and the mass relocation model. For ablation model, we used the neutral gas shielding (NGS) model, which most widely adopted in ablation models. The pellet ablation rate is described as

$$\frac{dN}{dt} = 1.12 \times 10^{16} n_e^{0.333} T_e^{1.64} r_p^{1.333} M_i^{-0.333} V_{\text{pel}}^{-1}, \quad (9)$$

where  $N$ ,  $n_e$ ,  $T_e$ ,  $r_p$ ,  $M_i$  and  $V_{\text{pel}}$  are the number of particles in a pellet, electron density, electron temperature, pellet radius, particle mass in pellet and injection velocity, respectively.

For mass relocation model, width from the ablation point with plasmoid drift in the major-radius direction  $\delta x$  ( $x = r/a$  is the normalized minor radius) is described as [14]

$$\delta x = \delta r/a \sim \delta \psi \Delta \psi, \quad (10)$$

where  $\psi$  is poloidal flux. The poloidal flux perturbation  $\delta \psi$  scaling is described as

$$\Delta \psi = q \beta B_t B_p^{-1} (1 + q L_e/a)^{-1} \times a^{-2} r_0^2 \delta n (n + \langle \delta n \rangle)^{-1}. \quad (11)$$

## 3. Simulation Results

### 3.1 Feasibility of pellet injection condition

In this study, we used the reactor parameters obtained from the reactor design system code PEC (Physics Engineering Cost) [4] as shown in Table 1. These parameters are derived from two 1-GW electric power fusion reactor designs; high-field, high-beta compact tokamak reactor TR-1 and high-beta helical system HR-1. The required alpha particle power in tokamak reactor should be greater than that in helical one. This is because the current drive power is required in the tokamak reactor.

An effectiveness of pellet injection from high magnetic field side (HFS) as shown in Fig. 1, has already been analyzed in the tokamak reactor [15]. Since HFS injection is a method of injecting a pellet from inner wall of reactor, it requires the use of curved guide tube to route the pellets from acceleration device. Therefore, the pellet speed is limited to ensure pellet survivability. An experi-

Table 1 Reactor parameters obtained from PEC code.

	$R_p$ (m)	$a_p$ (m)	$B_t$ (T)	$\kappa$	$\delta$	$I_p$ (MA)	$P_\alpha$ (MW)
TR-1(ITER like)	5.29	1.25	7.11	2.0	0.5	13.0	600
HR-1(LHD like)	16.8	2.8	4.21	-	-	-	470

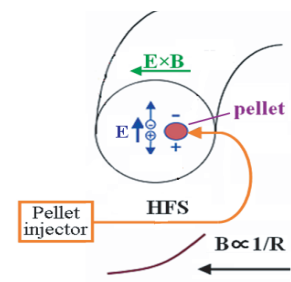


Fig. 1 Schematic of HFS pellet injection. Curved guide tube is required to route the pellet from pellet injector to inner wall of the torus equipment.

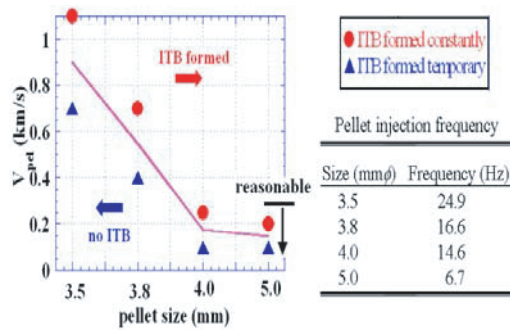


Fig. 2 Required  $V_{\text{pel}}$  and size for ITB formation. From the ITER curved guide tube experiment,  $V_{\text{pel}} < 0.3$  km/s is reasonable value at 5 mm $\phi$  pellet.

ment of the ITER guide tube installation for inner side pellet launch has been carried out at ORNL [16]. As a result of the experiment, it is shown that the pellet speed must be limited to 0.3 km/s for 5 mm $\phi$  pellet, which size is assumed as maximum size in ITER [17]. In this subsection, the feasibility of pellet injection condition for ITB formation is simulated in tokamak reactor.

Figure 2 shows the pellet speed required for ITB formation on tokamak reactor, TR-1. Pellets with size of 3.5 mm $\phi$ , 3.8 mm $\phi$ , 4.0 mm $\phi$  and 5.0 mm $\phi$  are simulated. Required pellet injecting frequency for each pellet size is also described. ITB could be formed at  $V_{\text{pel}} < 0.3$  km/s (limited speed of inner-side pellet injection in ITER) at 4 mm $\phi$  and 5 mm $\phi$  pellet. As for injection frequency, 10 Hz operation for 1,000 s has already been achieved with screw extruder type pellet injector used in LHD [15]. Therefore, from these results, in TR-1 class reactor, ITB can be formed under conditions of feasible pellet velocity, size and injection frequency.

### 3.2 ITB formation in tokamak and helical reactor

In this subsection, we made a comparison on ITB formation and core plasma profile between tokamak and helical reactors. For tokamak reactor, HFS injection using 4 mm $\phi$  or 5 mm $\phi$  pellet is simulated. In the helical case, since the effectiveness of HFS injection has not been observed so far [18] due to magnetic structure, we applied only NGS model as a pellet ablation model.

Figure 3 shows the radial profiles during steady state period of tokamak reactor using different pellet condition. The pellet size and  $V_{\text{pel}}$  for figures (a)(b), (c)(d) and (e)(f) are 4.0 mm $\phi$  - 0.3 km/s, 4.0 mm $\phi$  - 2.5 km/s and 5.0 mm $\phi$  - 0.3 km/s, respectively. Left figures show profiles of  $T_e$ ,  $n_e$ ,  $q$  and pellet density deposition  $\Delta n_e$ . Right figures show the improvement factor  $F(\omega_{E \times B} / \gamma_{\text{ITG}})$ ,  $\omega_{E \times B}$  and  $\gamma_{\text{ITG}}$  profiles. In each case, difference in the position of ITB formation did not appeared. ITB is formed at  $r/a \sim 0.6$ , where  $q$ -profile takes the minimum value. According to equation (4), the growth rate  $\gamma_{\text{ITG}}$  decreases at the  $q$  minimum posi-

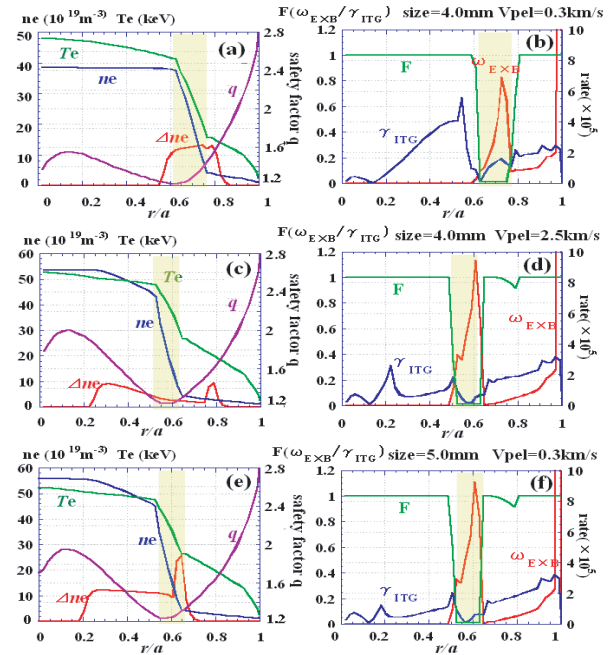


Fig. 3 Simulation results of tokamak reactor. Pellet size and  $V_{\text{pel}}$  for (a)(b), (c)(d), (e)(f) are 4 mm $\phi$  - 0.3 km/s, 4 mm $\phi$  - 2.5 km/s and 5 mm $\phi$  - 0.3 km/s, respectively. Left figures show electron temperature, electron density, pellet deposition and safety factor profiles in each cases, and figure right shows the improvement factor  $F(\omega_{E \times B} / \gamma_{\text{ITG}})$ ,  $\omega_{E \times B}$  and  $\gamma_{\text{ITG}}$  profiles.

tion ( $r/a \sim 0.6$ ), and the reduction of  $F(\omega_{E \times B} / \gamma_{\text{ITG}})$  occurs. This process leads to the ITB formation. Therefore, the position of ITB formation is not related to the penetration depth of the pellet injection. When the pellet is injected deeper up to  $r/a \sim 0.2$ , as shown in Figs. 3 (c) and (e), the electron density  $n_e$  in the plasma core is increased. Therefore, pellet injection has significant effect on the plasma radial profile in the tokamak reactor.

Figure 4 shows the simulation results during the steady state period of helical reactor. Profiles of  $T_e$ ,  $n_e$ ,  $\Delta n_e$  and  $E_r$  are shown in right figures depending on pellet size and velocity  $V_{\text{pel}}$ . In helical reactor case, ITB is formed more widely than that in tokamak reactor case at  $r/a \sim 0.1 - 0.3$ , where large  $E_r$  gradient locates. The  $n_e$  gradient increases where pellet ablation occurs. When the pellet is injected centrally as shown in Fig. 4 (c), compared with the case of pellet injection with shallow penetration as shown in Figs. 4 (a) and (e), the  $n_e$  gradient locates widely at the core region ( $r/a \sim 0.2 - 0.8$ ). Negative electric field in helical plasma is created by the ambipolar neoclassical flux, different from electric field formation mechanism in tokamak. These processes increase the  $\omega_{E \times B}$ , and leads to the  $F(\omega_{E \times B} / \gamma_{\text{ITG}})$  reduction in a wide range. This is the reason why ITB formed widely in helical reactor. In addition, in case of deeper pellet injection, average density value decreases due to the peaked  $n_e$  profile in a core region and central  $T_e$  increases. However, even the pellet injection

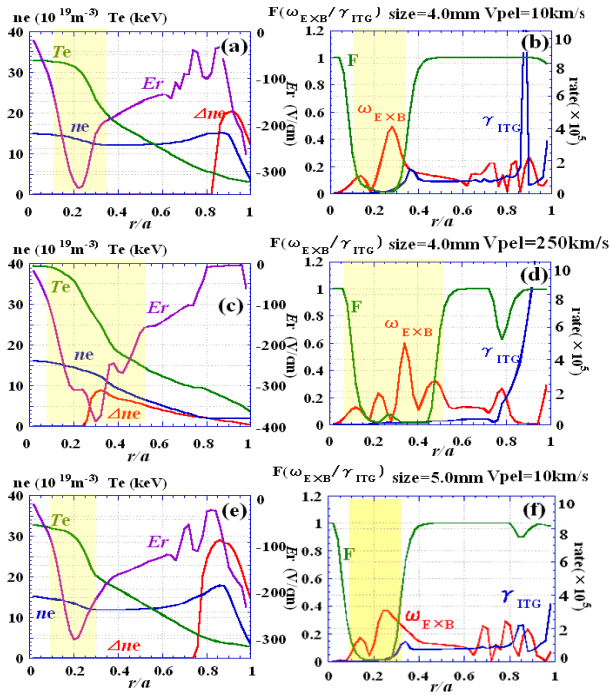


Fig. 4 Simulation results of helical reactor. Pellet size and  $V_{pel}$  for (a)(b), (c)(d) and (e)(f) are 4 mm $\phi$  - 10 km/s, 4 mm $\phi$  - 250 km/s and 5 mm $\phi$  - 10 km/s, respectively. Right figures show radial electric field,  $\omega_{E \times B}$  and  $\gamma_{ITG}$  profiles.

to core region is effective to form the wide-ranged ITB, it requires unrealistic velocity (250 km/s at 4 mm $\phi$  pellet) in the present technology.

#### 4. Summary

The feasibility of pellet injection condition from high

magnetic field side is clarified at the 1 GW-electric class TR-1 tokamak reactor. The plasma profile and ITB formation are simulated by changing pellet injection condition. The simulation results are compared with tokamak and helical cases. In both cases, it can be said that the depth of pellet injection has an effect to the radial density profile. In helical case, deep pellet injection makes the density gradient widely at the core region, and this leads to the formation of the wide-ranged ITB.

- [1] T. Tara *et al.*, Plasma Phys. Control. Fusion **43**, 507 (2001).
- [2] J. Garcia, K. Yamazaki, J. Dies and J. Izquierdo, Phys. Rev. Lett. **96**, 105007 (2006).
- [3] K. Yamazaki and T. Amano, Nucl. Fusion **32**, 633 (1992).
- [4] K. Yamazaki *et al.*, Fusion Eng. Des. **81**, 2743 (2006).
- [5] T.S. Hahm and K.H. Burrell, Phys. Plasmas **2**, 1648 (1995).
- [6] P. Zhou, W. Horton and H. Sugama, Phys. Plasmas **6**, 2503 (1999).
- [7] D.R. Ernst *et al.*, Phys. Plasmas **7**, 615 (2000).
- [8] Y.B. Kim, P.H. Diamond and R.J. Groebner, Phys. Fluids **B 3**, 2050 (1991).
- [9] F.L. Hinton and G.M. Staebler, Phys. Fluids B **5**, 1281 (1993).
- [10] B. Esposito *et al.*, Plasma Phys. Control. Fusion **45**, 933 (2003).
- [11] Y. Hori *et al.*, Plasma Fusion Res. **5**, S2034 (2010).
- [12] T. Fujita *et al.*, Phys. Rev. Lett. **78**, 2377 (1997).
- [13] T. Shimozuma *et al.*, Plasma Phys. Control. Fusion **45**, 1183 (2003).
- [14] A.R. Polevoi and M. Shimada, Plasma Phys. Control. Fusion **43**, 1525 (2001).
- [15] Y. Higashiyama *et al.*, Plasma Fusion Res. **3**, S1048 (2008).
- [16] S.K. Combs *et al.*, Fusion Eng. Des. **75**, 691 (2005).
- [17] R. Sakamoto and H. Yamada, NIFS-TECH-13 2005.
- [18] R. Sakamoto *et al.*, Proc. 29th EPS Conf. Plasma Phys. Contr. Fusion (Montreux, 2002), ECA Vol. **26B**, P-1.074 (2002).